LCGT Main Interferometer Design

LCGT Main Interferometer Working Group

February 21, 2011

Contents

Chapter 1

Design for bLCGT

We first present a preliminary design of the main interferometer for bLCGT.

1.1 Definition and Scope

The main interferometer (MIF) is a subsystem which is responsible for converting gravitational waves into electronic signals on a photodetector. It includes two arm cavities, the power recycling cavity and the signal recycling cavity. The MIF subsystem also provides specifications for output mode cleaner, which will be manufactured by the input/output optics group. In the LCGT's subsystem structure, this subsystem also includes the control system to keep the interferometer at the optimal operating point.

This subsystem provides no hardware because all the hardware which constitutes the main interferometer is provided by other subsystems, e.g. mirrors are provided by the mirror subsystem. What this subsystem provides is a design of the interferometer, which is transferred to other subsystems as specifications for their components. We are also mostly responsible for the commissioning of the interferometer once components are installed.

Here is a list of tasks we are assigned to:

- Determine the optical parameters of the main interferometer, except for the ones already determined by the detector configuration group.
- Determine the detailed optical layout of the main interferometer.
- Design robust length and alignment sensing schemes which do not contaminate the target sensitivity.
- Design a robust lock acquisition scheme.
- Make a commissioning plan to achieve the target sensitivity as soon as possible.

1.2 Requirements

- The main interferometer has to be able to achieve the target sensitivity of bLCGT (Figure 1.1). The target sensitivity of bLCGT is given by the fundamental noises estimated by the detector configuration group. All other technical noises has to be well below the fundamental noises.
- bLCGT has two operation modes: BRSE and DRSE. The main interferer configuration should allow us to switch between the two modes within a reasonable amount of time.

- The control schemes of the LCGT has to be robust enough to ensure stable operation of the interferometer in the environmental disturbances of Kamioka mine.

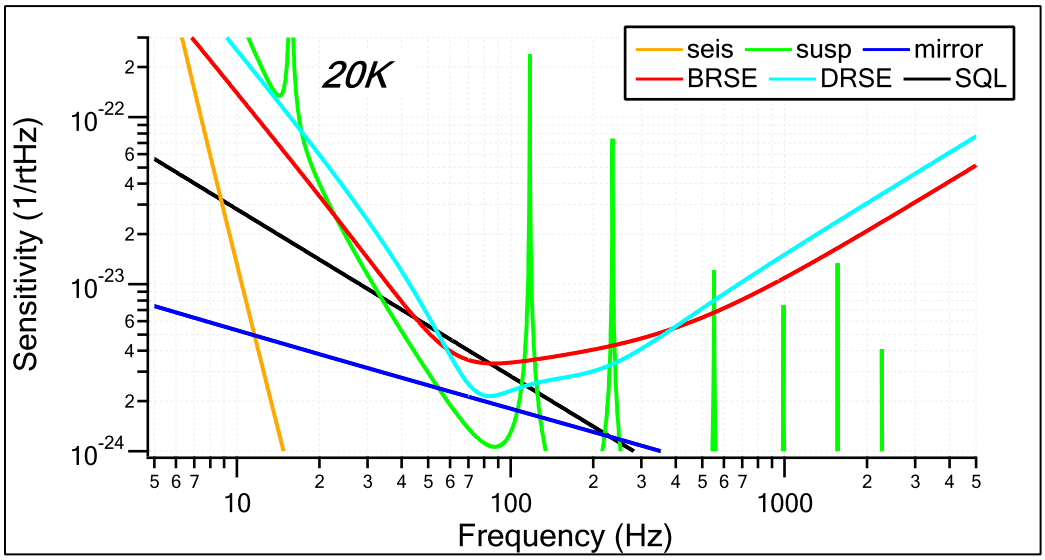

Figure 1.1: bLCGT Target Sensitivity

1.3 Interface

1.3.1 Mirror subsystem

Requirements to the mirror subsystem from MIF are listed in the tables 1.1 - 1.9.

1.3.2 Input/Output Optics Subsystem

Interface items with the input/output optics subsystem are listed in Table 1.10.

1.3.3 Suspension Subsystem

Interface items with the suspension subsystem are listed in Table 1.11.

1.3.4 Digital Subsystem

Interface items with the digital subsystem are listed in Table 1.12.

1.3.5 Analog Electronics Subsystem

Interface items with the analog electronics subsystem are listed in Table 1.13.

Parameter Name	Value	Comments
HR Reflectivity@1064 nm	99.6±0.01%	Power reflectivity
HR Reflectivity Mismatch @1064 nm	<0.05%	$\lvert R_{\mathrm{ITMX}} - R_{\mathrm{ITMY}} \rvert$
HR Reflectivity@532 nm	80±10%	ITM reflectivity must be smaller than ETM
HR loss@1064 nm	<45 ppm	Including diffraction and absorption
HR loss@532 nm	<1%	Including diffraction and absorption
AR Reflectivity@1064 nm	200(+100/-0) ppm	
AR Reflectivity@532 nm	<5%	
HR ROC	>500 km	As large as possible
HR ROC Mismatch between ITMX and ITMY	<10 km	
AR ROC	>500 km	As large as possible
AR Wedge Angle	0.2±0.002 deg	

Table 1.1: Input Test Mass Requirements

Parameter Name	Value	Comments
HR Reflectivity@1064 nm	>99.9945%	Power reflectivity
HR Transmissivity@1064 nm	>1 ppm	
HR Reflectivity@532 nm	80±10%	ETM reflectivity must be larger than ITM
HR loss@1064 nm	<45 ppm	Including diffraction and absorption
HR loss@532 nm	<1%	Including diffraction and absorption
AR Reflectivity@1064 nm	<1000 ppm	
AR Reflectivity@532 nm	No requirement	
HR ROC	7000±100 m	
HR ROC Mismatch between ITMX and ITMY	<7 m	
AR ROC	>100 km	As large as possible
AR Wedge Angle	0 deg	

Table 1.2: End Test Mass Requirements

Parameter Name	Value	Comments
HR Reflectivity@1064 nm	50±0.5%	S Polarization
HR Reflectivity@532 nm	<10%	As small as possible
AR Reflectivity@1064 nm	<50 ppm	
AR Reflectivity@532 nm	<10%	
HR ROC	>500 km	As large as possible
AR ROC	>500 km	As large as possible
AR Wedge Angle	0.383±0.002 deg	

Table 1.3: Beam Splitter Requirements

Parameter Name	Value	Comments
HR Reflectivity@1064 nm	90+0/-0.1%	
HR Loss@1064 nm	<100 ppm	
AR Reflectivity@1064 nm	<100 ppm	
HR ROC	300.6±1 m	
AR ROC	>100 km	As large as possible
AR Wedge Angle	2.0±0.1 deg	

Table 1.4: PRM Requirements

Parameter Name	Value	Comments
HR Reflectivity@1064 nm	85.0±1%	
HR Loss@1064 nm	<100 ppm	
AR Reflectivity@1064 nm	<100 ppm	
HR ROC	300.6±1 m	
AR ROC	>100 km	As large as possible
AR Wedge Angle	2.0±0.1 deg	

Table 1.5: SRM Requirements

Parameter Name	Value	Comments
HR Reflectivity@1064 nm	99.95±0.01%	
HR Reflectivity@532 nm	<10%	As small as possible
HR Loss@1064 nm	<100 ppm	
HR Loss@532 nm	<1%	
AR Reflectivity@1064 nm	<500 ppm	
AR Reflectivity@532 nm	<10%	
HR ROC	-3.251±0.01 m	
AR ROC	>50 km	As large as possible
AR Wedge Angle	2.0±0.1 deg	

Table 1.6: PR2 Requirements

Parameter Name	Value	Comments
HR Reflectivity@1064 nm	>99.99%	
HR Reflectivity@532 nm	>80%	As large as possible
HR Loss@1064 nm	<100 ppm	
HR Loss@532 nm	<1%	
AR Reflectivity@1064 nm	<1000 ppm	
AR Reflectivity@532 nm	No requirement	
HR ROC	27.36±0.1 m	
AR ROC	>10 km	As large as possible
AR Wedge Angle	2.0±0.1 deg	

Table 1.7: PR3 Requirements

Parameter Name	Value	Comments
HR Reflectivity@1064 nm	99.95±0.01%	
HR Reflectivity@532 nm	<10%	As small as possible
HR Loss@1064 nm	<100 ppm	
HR Loss@532 nm	<1%	
AR Reflectivity@1064 nm	<500 ppm	
AR Reflectivity@532 nm	<10%	
HR ROC	-3.251±0.01 m	
AR ROC	>50 km	As large as possible
AR Wedge Angle	2.0±0.1 deg	

Table 1.8: SR2 Requirements

Parameter Name	Value	Comments
HR Reflectivity@1064 nm	>99.99%	
HR Reflectivity@532 nm	>80%	As large as possible
HR Loss@1064 nm	<100 ppm	
HR Loss@532 nm	<1%	
AR Reflectivity@1064 nm	<1000 ppm	
AR Reflectivity@532 nm	No requirement	
HR ROC	27.36±0.1 m	
AR ROC	>10 km	As large as possible
AR Wedge Angle	2.0±0.1 deg	

Table 1.9: SR3 Requirements

Item	Value	Comments
Laser Power	85 W at PRM input	Carrier Power
Modulation Frequencies	16.875 MHz, 45 MHz, 39.375 MHz, 56.25 MHz	see section 1.6
Modulation Depth	max 0.3	
Mode Cleaner Length		
Laser Frequency Noise	TBD	
Laser Intensity Noise	TBD	
Frequency Actuation	TBD	
Output Mode Cleaner	TBD	
Mode Matching Telescopes	TBD	
Beam Reducing Telescopes	POX, POY, TRX, TRY	
Green Lasers	TBD	

Table 1.10: Interface Items with the Input/Output Optics Subsystem

Item	Value	Comments
Vibration Isolation Performance for Type A SAS	3×10^{-20}m/$\sqrt{\text{Hz}}$@10 Hz	see section 1.6.5
Vibration Isolation Performance for Type B SAS	1.5×10^{-17}m/$\sqrt{\text{Hz}}$@10 Hz	see section 1.6.5
Adjustable Range of Mirror Locations	TBD (in the order of a few cm)	After the installation of the mirrors, the locations must be adjusted to compensate for ROC errors.
Actuation Range	TBD	
Local Sensors	TBD	

Table 1.11: Interface Items with the Suspension Subsystem

Item	Value	Comments
Sampling Frequency	max 64 kHz	
ADC dynamic range	80 dB	This requirement comes from lock acquisition

Table 1.12: Interface Items with the Digital Subsystem

Item	Value	Comments
Maximum Power on PDs	>100 mW	
Maximum RF PD Frequency for observation	60 MHz	
Maximum RF PD Frequency for lock acquisition	135 MHz	
Maximum RF QPD Frequency	60 MHz	

Table 1.13: Interface Items with the Analog Electronics Subsystem

Item	Value	Comments
Optical Layout		see section 1.5
View Ports	TBD	

Table 1.14: Interface Items with the Vacuum Subsystem

Item	Value	Comments
Length of radiation shield	20 m	
Location of holes in the radiation shield baffles for POX and POY		see section 1.5

Table 1.15: Interface Items with the Cryogenic Subsystem

1.3.6 Vacuum Subsystem

Interface items with the vacuum subsystem are listed in Table 1.14.

1.3.7 Cryogenic

Interface items with the cryogenic subsystem are listed in Table 1.15.

1.4 Optical Configuration

1.4.1 Overview

The main interferometer part of bLCGT is a dual recycled Fabry-Perot Michelson interferometer operating in a resonant-sideband extraction (RSE) mode. The schematic view of the main interferometer and the naming convention of the interferometer components are shown in Figure 1.2.

1.4.2 Arm Cavity

The arm cavity length is constrained to less than 3 km by the size of the mountain. So we chose the largest one. The reflectivities of the mirrors are set by the detector configuration group to optimize the sensitivity under the constraint that the heat absorption at ITM should not exceed the cooling power of the cryogenic system. This constraint led us to choose a relatively high finesse and a high RSE gain.

The radius of curvature of the mirrors are chosen by considering the following factors.

- The beam spot size should not be too large to induce more than 1 ppm of diffraction loss.
- The beam spot size should not be too small to make the coating thermal noise too large.
- The g-factor of the cavity should be stable enough, i.e. higher order spatial modes should not resonate in the arm cavity at the same time as the fundamental mode.
- The parametric instability must be avoided.

Arm cavity parameters are listed in Table 1.16. Detailed reasoning behind the choice of the parameters is given in appendix A.2.

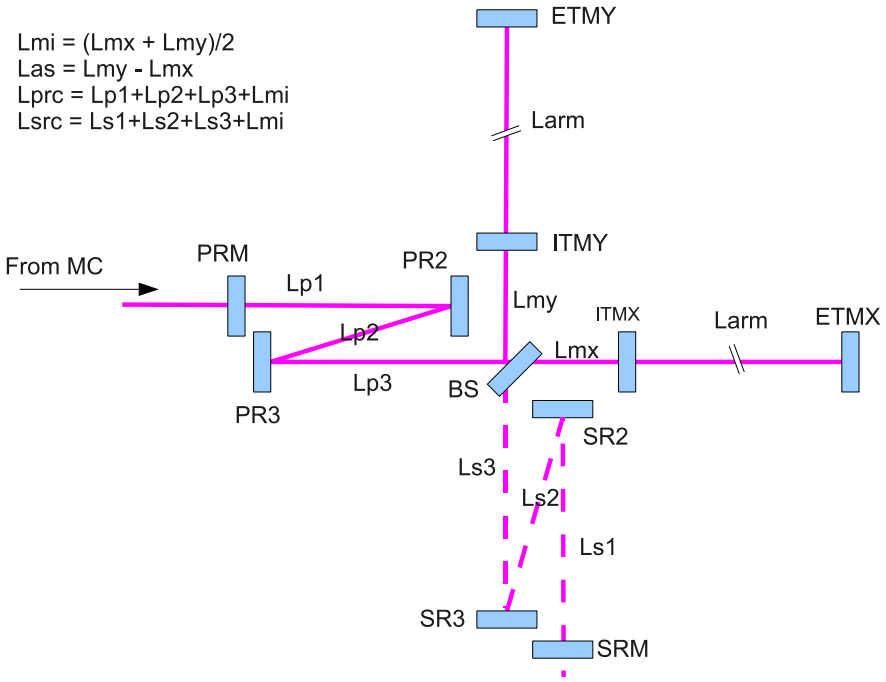

Figure 1.2: Schematic of the main interferometer and the naming convention of IFO parameters

Parameter Name	**Value**	**Comments**
Arm cavity length	3000.00 m	
ITM Reflectivity	99.6%	
ITM Radius of Curvature	flat (>500 km)	
ITM Beam Size	3.43 cm	$1/e^2$ radius
ETM Reflectivity	99.9945%	
ETM Radius of Curvature	7000 m	
ETM Beam Size	4.53 cm	$1/e^2$ radius
g-factor	0.572	$\sqrt{g_1 \cdot g_2}$
Round Trip Loss	<100 ppm	
Finesse	1546	

Table 1.16: Arm cavity parameters

1.4.3 Recycling Cavities

The reflectivities of the recycling mirrors are determined by the detector configuration group to optimize the power and signal recycling gain.

The length parameters of the recycling cavities (RCs) are set to resonate the RF sidebands used for the control signal extraction, which is explained in section 1.6. There are two RF sidebands entering the power recycling cavity (PRC), called f1 and f2. The Schnupp asymmetry of the Michelson part (MICH) is chosen to perfectly reflect the f2 sideband by MICH, so that f2 does not see the signal recycling cavity (SRC). The f1 sideband transmits through MICH and resonates in the compound cavity formed by PRC and SRC through MICH.

The actual length of the recycling cavities have to be fine adjusted to fully resonate the f1 and f2 sidebands, because f1 and f2 get non-zero phase shift when reflected by the arm cavities. This is achieved by fine tuning the f1 and f2 frequencies so that the reflection phases of those sidebands to the arm cavities have the ratio of f1:f2. The mode cleaner length and the recycling cavity lengths are adjusted accordingly.

The average length of MICH (the average distance between BS and ITMs) is set to 25 m. Out of this 25 m, 20 m is used for the cryogenic radiation shield, which protects the cryogenic ITMs from 300 K thermal radiation of the BS chamber. The remaining 5m is used to absorb the Schnupp asymmetry.

The recycling cavities are both folded by two additional mirrors to allow focusing of the beam inside the cavities. This configuration makes the recycling cavities stable in terms of spatial modes. However, the recycling cavities cannot be too stable, because then TEM10 or TEM01 modes generated by the misalignment of the arm cavities will be suppressed in the RCs. Those higher order modes are necessary for the alignment sensing by the wavefront sensing (WFS) scheme. The one-way Gouy phase change of the TEM00 beam resonating in either recycling cavities is set to 20 deg. as a compromise between the stability of the RCs and the WFS signal strength. The ROCs of the folding mirrors are set to realize the Gouy phase shift.

The geometry of the folding part is mainly determined by the constraints from the vacuum system, such as the minimum separation between vacuum chambers. In order to minimize the astigmatism, we chose a configuration which minimizes the folding angle under the constraints. The beam from PR3 to BS has a large radius (3.5 cm). Therefore, PR2 has to be located far enough from the beam to avoid beam clipping. On the other hand, we want to put PR2 as close to the beam as possible to minimize the astigmatism. As a result, we located the edge of PR2 at 4 times the beam radius away from the beam.

1.5 Optical Layout

The exact locations and the orientations of the interferometer mirrors have to be determined to satisfy the following criteria:

- X-arm and Y-arm are orthogonal.
- Beams hit the mirrors at the center.
- Recycling cavity lengths and the Schnupp asymmetry match the designed values including the optical distance of the transmissive optics.

Since some optics have AR wedge, it is not a trivial task to trace the beams through the interferometer and find a configuration which satisfy the above conditions. Doing it manually is also an error-prone process. We also have to track unwanted reflections from the AR surfaces to appropriately damp the stray beams. This is also a daunting task. Therefore, we developed a Python library, called gtrace, for

Parameter Name	Value	Comments
Power Recycling Cavity Length	66.591 m	
Signal Recycling Cavity Length	66.591 m	
Michelson Average Length	25.0 m	
Michelson Asymmetry	3.330 m	
PRM Reflectivity	90%	
PRM ROC	300.624 m	
PRM Beam Size	4.05 mm	$1/e^2$ radius
PR2 ROC	-3.251 m	
PR2 Beam Size	4.05 mm	$1/e^2$ radius
PR3 ROC	27.36 m	
PR3 Beam Size	34.25 mm	$1/e^2$ radius
PRM Reflectivity	84.64%	
SRM ROC	300.624 m	
SRM Beam Size	4.05 mm	$1/e^2$ radius
SR2 ROC	-3.251 m	
SR2 Beam Size	4.05 mm	$1/e^2$ radius
SR3 ROC	27.36 m	
SR3 Beam Size	34.25 mm	$1/e^2$ radius

Table 1.17: Recycling cavity parameters

Parameter Name	Value	Comments
Lp1	14.761 m	Distance between PRM and PR2
Lp2	12.067 m	Distance between PR2 and PR3
Lp3	14.764 m	Distance between PR3 and BS
Ls1	14.761 m	Distance between SRM and SR2
Ls2	12.067 m	Distance between SR2 and SR3
Ls3	14.764 m	Distance between SR3 and BS
Folding Angle	0.6293 deg	The incident angle to the folding mirrors.

Table 1.18: Folding parameters. See Figure 1.2 for the meaning of the parameters.

tracing beam paths and the evolution of Gaussian beam parameters through the interferometer. Detailed optical layout of LCGT main interferometer is automatically generated by a Python code given a set of interferometer parameters (distance between the mirrors, mirror properties etc) and constraints.

The optical layout generation code and the generated CAD files are available in the LCGT svn [1].

1.5.1 Tunnel Slope

One thing to be kept in mind here is the tunnel slope. Since the 3 km tunnels of LCGT are slightly tilted for water drainage, the two arms are not on a level plane. We decided that all the main interferometer optics be placed on the plane defined by the two arms. This plane is tilted with respect to the local gravitationally level plane. The optical layout generated by the above code is drawn on this tilted plane. In the actual construction and the installation of the vacuum chambers, the optical layout has to be projected from the tilted plane to the reference plane used for the construction.

1.6 Length Sensing and Control Scheme

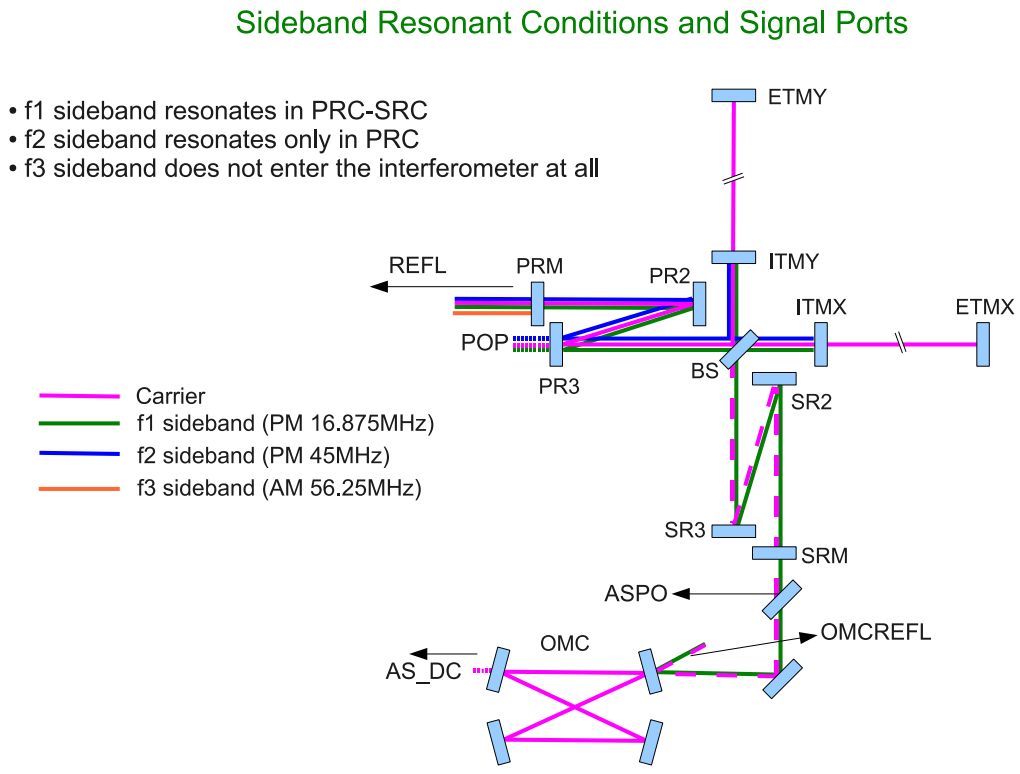

Figure 1.3: RF sideband resonant conditions and signal ports. POP is drawn at the transmission of PR3 to avoid congestion of the diagram. However, POP is actually planned to be picked up from the back of PR2 because the beam size is much smaller there.

f1	16.880962 MHz	$3 \times f_{\rm MC}$, PM
f2	45.015898 MHz	$8 \times f_{\rm MC}$, PM
f3	39.388910 MHz and 56.269873 MHz	$7 \times f_{\rm MC}$ and $10 \times f_{\rm MC}$, AM
$f_{\rm MC}$	5.626987 MHz	MC FSR
$L_{\rm MC}$	26.6388 m	MC Length

Table 1.19: RF Sideband Frequencies

1.6.1 Overview

The length degrees of freedom to be controlled are DARM, CARM, MICH, PRCL and SRCL (see appendix B for the definitions of the acronyms). DARM is sensed at the AS port by the DC readout scheme. Other degrees of freedom are sensed by a variant of frontal modulation scheme. The input laser beam is phase or amplitude modulated to generate RF sidebands. There are two RF sidebands, which resonate in the central part (PRC, MICH, SRC) of the interferometer. The sideband resonant conditions are shown in Figure 1.3. The f1 sideband resonates in the compound cavity of PRC-SRC. The MICH reflectivity to the f2 sideband is chosen to be almost 100%. Consequently, f2 only resonates in PRC. Optionally, we may add another RF sideband, f3, which does not enter the interferometer at all. f3 is called non-resonant sideband (NRS).

When operated in DRSE configuration, the detuning of the SRC is done by adding offset to the error signal of SRCL. The required detuning of SRC is 3.5 degree in terms of the one-way phase shift of SRCL, which corresponds to 10 nm shift of SRM position. The f1 sideband frequency is chosen to make the resonance of f1 to SRC not too sharp, so that the detuned SRC can still produce a reasonable error signal using f1. The SRCL error signal is plotted as a function of SRM position in Figure 1.4. The operating point of DRSE has enough slope to produce strong error signal. However, the non-linearity of the error signal is stronger at the DRSE operating point. Discussions on this non-linearity and other issues with the offset detuning of SRC can be found in Appendix A.

The selected RF modulation frequencies are listed in Table 1.19. The mode cleaner has to transmit the RF sidebands. For this reason, the FSR of the MC is chosen to be f2/8.

Simulation Codes The calculations shown in the following sections are all done by using a simulation tool called Optickle [2]. The interferometer model and simulation codes are available in the LCGT svn at [3].

1.6.2 Signal Name Convention

In this document, signal names follow the convention described here. A signal name consists of a port name followed by an indicator of demodulation scheme connected with an underscore (_). For example, "REFL_1I" means a signal detected at the reflection port and demodulated at the f1 frequency in I-phase. Another example is "AS_DC", which means a DC signal detected at the AS port.

Double demodulation may be used if we use the f3 sideband. In this case, a signal name looks like "REFL_1DmQ". This means a signal detected at the REFL port demodulated at f3-f1 frequency in Q-phase. Double demodulation is always between f3 and one of the other SBs. Therefore, only one number is specified. The letter "D" means double demodulation, "m" means f3 minus f1. In the case of f3 plus f1, this letter will be "p".

"REFL_1DmQ" is not a true double-demodulation, where the signal should be demodulated twice at f3 and f1 frequencies. However, it carries similar information as the true double-demodulation.

	DARM	CARM	MICH	PRCL	SRCL
AS_DC	1	4.2×10^{-5}	1.0×10^{-3}	4.8×10^{-6}	4.7×10^{-6}
REFL_1I	5.4×10^{-3}	1	4.3×10^{-5}	6.5×10^{-3}	4.3×10^{-3}
REFL_1Q	5.0×10^{-3}	1.3×10^{-2}	1	1.02	0.67
POP_2I	2.3×10^{-2}	4.3	1.0×10^{-2}	1	2.5×10^{-4}
POP_1I	8.7×10^{-2}	16.2	3.1×10^{-2}	2.1	1

Table 1.20: Normalized Sensing Matrix of LSC in the case of BRSE. Each row is normalized by the diagonal element. The interferometer response was evaluated at 100 Hz to create this matrix.

	DARM	CARM	MICH	PRCL	SRCL
AS_DC	1	4.1×10^{-5}	1.0×10^{-3}	4.5×10^{-6}	7.6×10^{-6}
REFL_1I	1.2×10^{-2}	1	1.3×10^{-4}	1.2×10^{-2}	1.4×10^{-3}
REFL_1Q	2.8×10^{-2}	9.9×10^{-3}	1	0.39	0.18
POP_2I	2.7×10^{-2}	4.3	1.0×10^{-2}	1	8.5×10^{-5}
POP_1I	1.7×10^{-1}	35	3.1×10^{-2}	2.0	1

Table 1.21: Normalized Sensing Matrix of LSC in the case of DRSE. Each row is normalized by the diagonal element. The interferometer response was evaluated at 100 Hz to create this matrix.

1.6.3 Signal Extraction Ports

The default length sensing scheme for bLCGT uses two phase modulated RF sidebands, f1 and f2. Beat signals of these sidebands with the carrier are detected at REFL and POP to extract necessary error signals. The signal sensing matrix for this scheme in the case of BRSE operation is shown in Table 1.20.

CARM signal produces large non-diagonal elements to the PRCL and SRCL. This is because the phase change of the carrier by CARM is usually much larger than that of the RF sidebands by PRCL or SRCL. However, CARM loop can have a very large control gain because of the very fast nature of the laser frequency feedback. We can rely on this fact to suppress the interference of CARM to PRCL and SRCL.

In REFL_1Q, the mixture of PRCL and SRCL to MICH is large. This does not happen when there is no asymmetry in the interferometer. When calculating the sensing matrix, we introduced 1% asymmetry[1] between the two arms. This asymmetry makes the CARM, PRCL and SRCL signals no longer be at exactly the orthogonal quadrature to the MICH signal. In the case of Table 1.20, we chose a demodulation phase which minimizes the coupling of CARM. In return, the PRCL and SRCL signals became comparable to MICH. However, these signals cab be separated because the lower right 3×3 matrix of Table 1.20 is invertible.

The sensing matrix for DRSE operation is shown in Table 1.21.

If we use the f3 sideband, which is an AM non-resonant sideband, the sensing matrix looks like Table 1.22 (BRSE). The large CARM interference disappeared in this case. So we don't have to rely on the gain hierarchy. However, in this configuration, we have to introduce a Mach-Zehnder interferometer at the modulation stage to separate the AM generation path and the PM generation path. This is necessary to avoid the generation of sub-sidebands at the double demodulation frequencies. This addition of Mach-Zehnder may introduce additional noise.

[1] Not the Schnupp asymmetry.

	DARM	CARM	MICH	PRCL	SRCL
AS_DC	1	4.1×10^{-5}	1.0×10^{-3}	4.8×10^{-6}	4.7×10^{-6}
REFL_1I	5.4×10^{-3}	1	3.9×10^{-5}	5.4×10^{-3}	4.5×10^{-3}
REFL_1DmQ	4.8×10^{-3}	2.5×10^{-3}	1	0.7	1.3×10^{-3}
REFL_2DmI	1.83×10^{-3}	8.3×10^{-2}	0.18	1	0.32
REFL_1DmI	2.5×10^{-4}	1.5×10^{-2}	2.4×10^{-2}	1.7	1

Table 1.22: Normalized Sensing Matrix of LSC for BRSE using the f3 sideband. Each row is normalized by the diagonal element. The interferometer response was evaluated at 100 Hz to create this matrix.

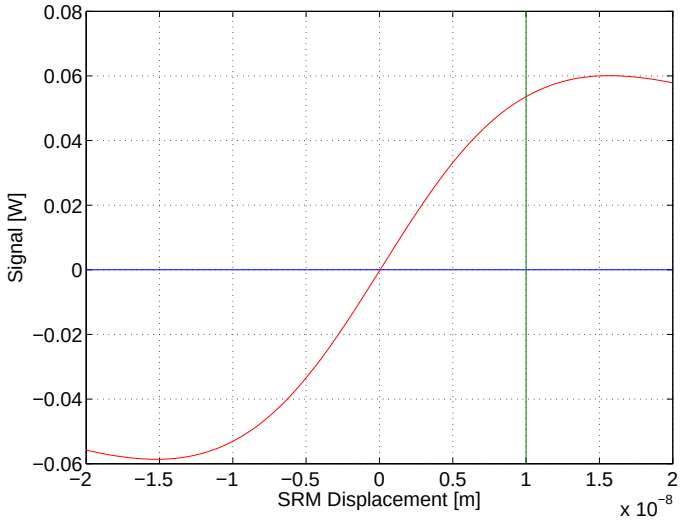

Figure 1.4: SRCL error signal as a function of SRM position. The green vertical line indicates where the SRM should be when operated in DRSE configuration.

1.6.4 Loop Noise

In general, the auxiliary degrees of freedom have larger shot noise than DARM. By using those signals for mirror control, we are effectively injecting noise into the interferometer. Especially, MICH has an unavoidable coupling to DARM by about 1/Finesse. Therefore, the shot noise of the MICH error signal appears to DARM attenuated by that factor. This is noise coupling mechanism is called loop noise.

The shot noise coupling by the control loops was calculated by assuming the unity gain frequencies shown in Table 1.23. The MICH UGF for DRSE is lowered to 10 Hz to further reduce the noise coupling.

	BRSE	**DRSE**
DARM	200 Hz	200 Hz
CARM	10 kHz	10 kHz
MICH	50 Hz	10 Hz
PRCL	50 Hz	50 Hz
SRCL	50 Hz	50 Hz

Table 1.23: Control Loop UGFs

The loop noise contributions from the auxiliary degrees of freedom are shown for the BRSE case in Figure 1.5. The curve labeled DARM is the target quantum noise level. It is clear that loop noise couplings from other degrees of freedom are larger than the target level.

The loop noise coupling can be reduced by a technique called feed forward [4]. Its working principle is the following. Taking PRCL as an example, we can measure the transfer function from the motion of PRM to the DARM signal. Then we assume that the error signal of PRCL is dominated by shot noise (or any sensing noise). This means that PRM is moved according to the shot noise by the feedback. From the feedback signal, we know exactly how much the PRM is erroneously moved. Therefore, we can predict how much noise is injected from this PRM motion to DARM with the knowledge of the above mentioned transfer function. By feeding forward this information to DARM, we can subtract the loop injected noise. The quality of feed forward is measured by the accuracy of the subtraction. Feed forward gain is defined as the inverse of the accuracy. If the accuracy is 1%, the feed forward gain is 100.

In Figure 1.6, the loop noise couplings are shown when the feed forward is applied with the gain of 100 to MICH, PRCL and SRC. With the feed forward, the loop noise couplings are well below the DARM quantum noise. The loop noise coupling with the feed forward for the case of DRSE is shown in Figure 1.7. Again, the loop noise is not a problem.

1.6.5 Displacement Noise Requirement

One caveat of feed forward is that it can increase the displacement noise coupling of the auxiliary degrees of freedom to DARM. Feed forward assumes that whatever you see in the error signal of an auxiliary degree of freedom, say PRC, is sensing noise, i.e. not a real motion of the mirror. This assumption is not valid in some frequencies. If the error signal reflects real motion of the mirror, this motion is suppressed by the feedback. Feeding forward this error signal to DARM means that you are trying to cancel the motion of the mirror (PRM) which is already suppressed by the (PRCL) feedback. The net result of this is the injection of the displacement noise of the auxiliary degrees of freedom into DARM.

One can calculate the transfer functions from the motion of auxiliary degrees of freedom to DARM with the feedback and the feed forward engaged. By requiring the displacement noise couplings to be a factor of 10 below the quantum noise of DARM, we can deduce the requirements to the displacement noise for each degrees of freedom. The calculated displacement noise requirements are shown in Fig-

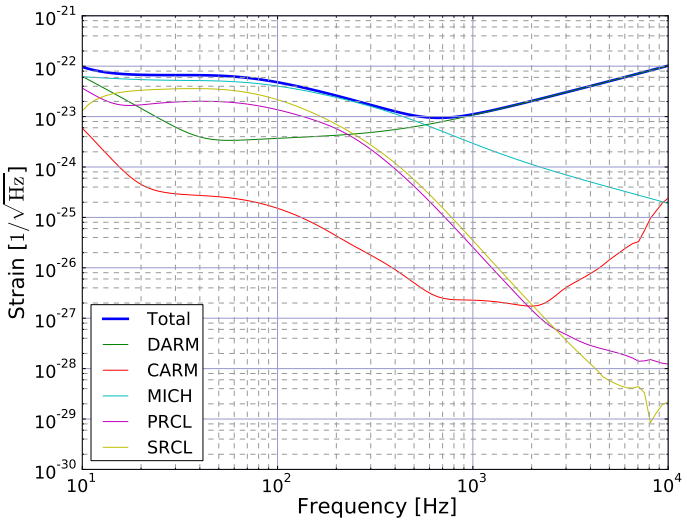

Figure 1.5: Loop Noise Coupling: BRSE

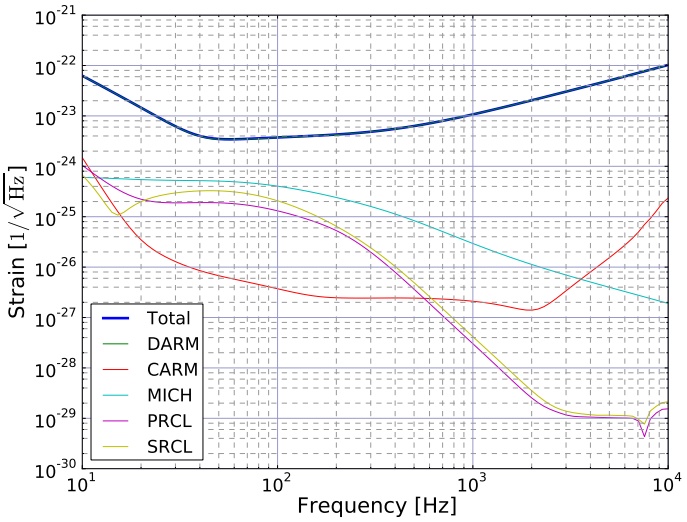

Figure 1.6: Loop Noise Coupling with Feed Forward: BRSE

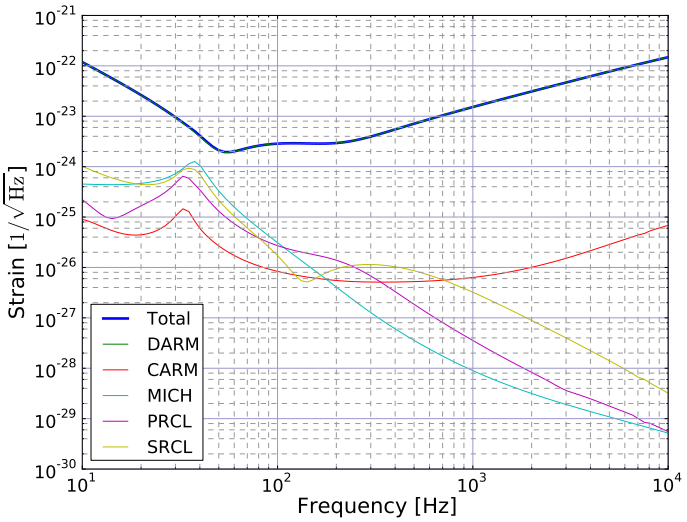

Figure 1.7: Loop Noise Coupling with Feed Forward: DRSE

ure 1.8 (BRSE) and Figure 1.9. The line labeled "SAS noise" in the plots is a simplified noise model of Type A SAS. The Type A SAS performance satisfies the displacement noise requirements of all mirror.

1.7 Alignment Sensing and Control Scheme

1.8 Overview

The alignment sensing and control (ASC) scheme of bLCGT has not yet fully determined. We plan to use a combination of the wave front sensing (WFS) scheme and optical levers. Currently we are studying the sensing matrix of WFS with an Optickle model[2]. A preliminary sensing matrix is shown in Figure 1.10.

The WFS signals are sensed in the soft-hard mode basis in terms of the radiation pressure [5]. CS, CH, DS and DH in the sensing matrix mean, "Common Soft", "Common Hard", "Differential Soft" and "Differential Hard" respectively.

1.9 Lock Acquisition Scheme

1.9.1 Overview

Quick and robust lock acquisition is important for maintaining high duty cycle. The lock acquisition procedure of bLCGT proposed here consists of three stages. First, the arm cavities are locked by green lasers at off-resonant positions for the main laser carrier. Then the central part of the interferometer is locked either by using the third harmonics demodulation signals or non-resonant sideband. Finally, the arm cavities are brought to full resonance to the main laser by changing the relative frequency of the

[2]In particular, we are using the Pickle package developed by Lisa Barsotti.

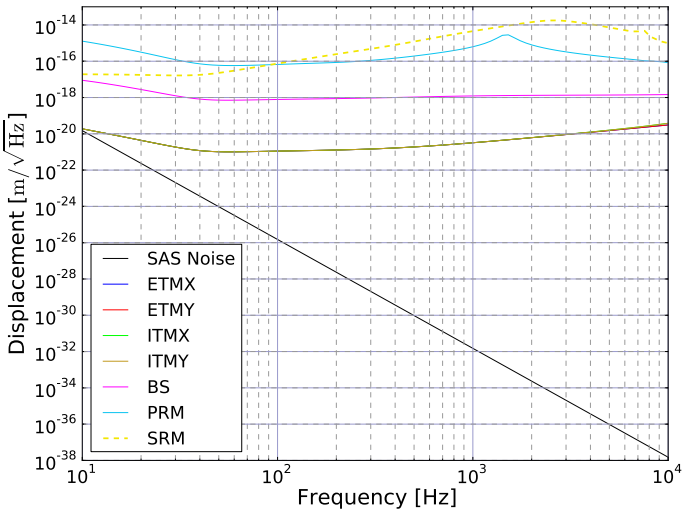

Figure 1.8: Displacement Noise Requirement for Each Mirror: BRSE, SDM

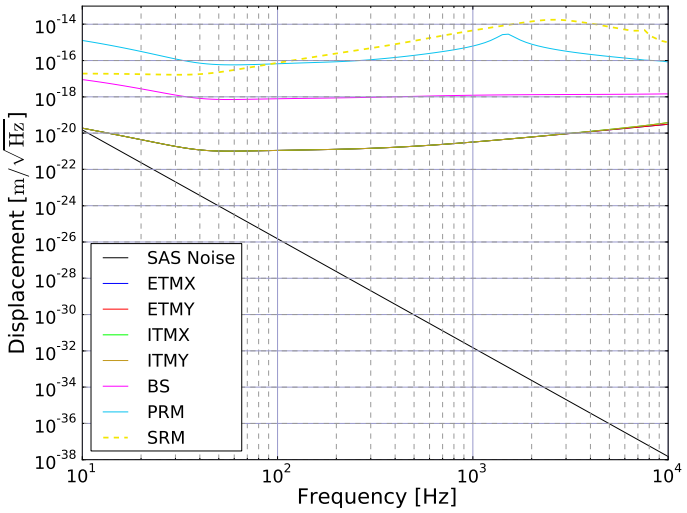

Figure 1.9: Displacement Noise Requirement for Each Mirror: DRSE, SDM

Angle Sensing Matrix [W/rad]

	CS	CH	DS	DH	PRM	PR2	PR3	SRM	SR2	SR3	BS
POY_B Q2	-31	28	-102	108	2.57	25.4	212	0.00362	0.00689	0.0577	-196
POY_B I2	-688	985	-1.68e+003	2.05e+003	60.2	718	6.12e+003	-0.00255	-0.00484	0.0406	-2.69e+003
POY_A Q2	37.4	-53.8	-56.5	43.9	-3.28	-39.2	-334	-0.00247	-0.0047	-0.0394	-9.1
POY_A I2	-129	135	1.6e+003	-1.74e+003	7.44	0.255	70.7	-0.0154	-0.0293	-0.245	4.28e+003
POY_B Q1	47	-24	-77.9	53.6	-1.98	-15.9	-129	-4.89	-9.29	-77.9	-236
POY_B I1	52.6	-51.2	-55.5	61.4	5.3	47.7	394	-0.72	-1.37	-11.5	295
POY_A Q1	115	-150	-114	148	-10.7	-117	-984	0.826	1.57	13.2	-691
POY_A I1	193	-33.4	-201	57.3	-8.65	-94	-791	-7.8	-14.8	-124	-603
POX_B Q2	739	-810	450	-711	-61.9	-668	-5.63e+003	0.0126	0.0239	0.2	3.52e+003
POX_B I2	-680	761	-236	439	-57	-621	-5.24e+003	0.015	0.0286	0.239	-2.75e+003
POX_A Q2	35.8	-18.9	-102	130	-2.76	-23.6	-194	-0.00164	-0.00311	-0.0261	-235
POX_A I2	87.5	-380	-1.74e+003	1.94e+003	-11	-201	-1.77e+003	-0.0118	-0.0225	-0.189	-5.39e+003
POX_B Q1	-132	59.2	-101	14.5	5.47	70.1	599	2.27	4.33	36.2	-108
POX_B I1	-52.8	79.8	-59.6	92.4	4.45	58.9	504	-1.1	-2.1	-17.6	-17.5
POX_A Q1	180	-36.2	195	-76.3	-8.73	-92.6	-777	-7.43	-14.1	-118	62.7
POX_A I1	87.7	-134	84.4	-127	-9.17	-98	-824	1.87	3.55	29.8	17.7
POP_B Q2	30.9	-27.7	0.0835	-0.107	-2.57	-25.3	-212	5.64e-006	1.07e-005	8.99e-005	-74.6
POP_B I2	698	-995	-1.76	2.12	-61.2	-728	-6.2e+003	-0.000115	-0.00022	-0.00184	-2.19e+003
POP_A Q2	-18.9	135	0.569	-0.589	3.01	65.6	582	1.24e-005	2.36e-005	0.000197	206
POP_A I2	63.4	-188	-0.585	0.451	-2.09	-52.7	-509	-1.01e-005	-1.92e-005	-0.000161	-182
POP_B Q1	18.7	-42.4	14.4	-18.4	-0.449	-5.82	-50	-4.6	-8.74	-73.2	-35.6
POP_B I1	-4.31	8.45	69.6	-87.5	0.0635	0.93	8.06	0.956	1.82	15.2	205
POP_A Q1	0.796	0.931	155	195	-0.055	-0.594	-5.01	0.000227	0.000432	0.00362	-452
POP_A I1	-82.2	64	-0.395	0.193	0.423	4.12	33.7	-6.81	12.9	109	12.7
AS_B Q1	-18.2	22.1	-173	272	1.63	14.2	117	-0.216	-3.84	-34.6	20.2
AS_B I1	114	-139	2.31e+003	-3.18e+003	5.71	62.5	526	3.34	36.1	333	-394
AS_A Q1	14.4	-43.2	1.04e+004	-7.96e+003	2.05	19.9	166	-1.05	-5.15	-47.2	-924
AS_A I1	54.8	-29.3	1.63e+004	-1.24e+004	3.55	45.1	385	1.35	8.59	78.4	-1.77e+003
REFL_B Q2	1.95e+003	8.46e+003	-21.4	22	816	4.12e+003	3.64e+004	0.000779	0.00148	0.0124	1.29e+004
REFL_B I2	865	-4.23e+003	10.7	-10.9	-406	-2.01e+003	-1.78e+004	-0.000372	-0.000707	-0.00593	-6.32e+003
REFL_A Q2	-426	114	-1.52	2.32	-6.78	235	1.89e+003	-4.03e-005	-7.66e-005	-0.000642	660
REFL_A I2	1.08e+004	9.78e+003	8.32	-14.8	872	561	655	0.000125	0.000239	0.002	520
REFL_B Q1	122	-182	318	-400	21	0.00182	-63.6	-7.01	-13.3	-112	927
REFL_B I1	-380	567	96.9	-121	-63.3	-0.0692	193	23.6	44.8	376	293
REFL_A Q1	37.8	-40	943	-1.18e+003	3.93	0.522	15.9	0.00878	0.0167	0.14	2.76e+003
REFL_A I1	1.84e+003	1.46e+003	-11.8	13.8	-110	-1.8	685	40.6	77.3	648	182

Figure 1.10: Preliminary sensing matrix for ASC. A and B in the signal name denotes two different Gouy phases.

green lasers to the main laser. After all the degrees of freedom are brought to the operation points, the error signals are switched to the ones with good shot noise.

The control signals for the central part can be disturbed by the arm cavities if one of the RF sidebands accidentally resonates in the arm cavities. Free hanging mirrors move around and randomly pass by the resonances of the RF sidebands. This makes the lock acquisition very difficult and an non-deterministic process. For this reason, we will pre-lock the arm cavities at a off-resonant position. The pre-lock position is off-resonant to the carrier because if pre-locked at the full resonance, a huge increase of the carrier power induces a radiation pressure thrust to the mirrors when the PRC is locked. To avoid this shock, the arms are first locked to off-resonance.

After locking the central part, the arm offset is slowly reduced to bring them to the full resonance. During this process, the error signals to lock the central part may be affected. Especially, the single demodulation signals are strongly affected by the large change of the carrier power and phase. Therefore, these signals are not suitable for the lock acquisition. We will use either the third harmonics demodulation signals or the double-demodulation signals with NRS for the lock of the central part during the lock acquisition.

1.9.2 Green Laser Pre-Lock

In order to lock the arms at off-resonance of the carrier, we will use phase locked green lasers. Two frequency doubled 532 nm lasers are used. The seed lasers (1064 nm) for those green lasers are phase locked to the main laser carrier with a PLL. Using this PLL, we can sweep the relative frequency of the green lasers to the main laser.

The arm cavity mirrors are dichroic coated to have some reflectivities to 532 nm, forming a low finesse cavity. Each arm cavity is locked to a green laser by the usual PDH scheme. By sweeping the green laser frequency relative to the main laser, the resonant condition of the arm cavities to the main carrier can be changed smoothly.

The injection points of the green lasers are shown in Figure 1.11. The green laser beams are injected from the back of PR2 (for X-arm) and SR2 (for Y-arm). PR2 is chosen over PR3 because the beam size at PR2 is about 4 mm, which is more manageable compared to 3.5 cm at PR3.

PR2 and PR3 are dichroic coated to have a good transmittance to 532 nm. PR3 and SR3 should have high reflectivities to the green beam, whereas BS should have a high transmittance. Therefore, the beam injected from PR2 mainly reaches the X-arm and the one from SR2 sees only the Y-arm. Of course, the beam separation is not perfect, especially considering that it is difficult to put high spec coatings for 532 nm keeping the coating performance for 1064 nm. Since we do not want to compromise on the performance of the coatings for 1064 nm, we relaxed the requirements for 532 nm, so that the coating company can optimize the coatings mainly for 1064 nm. The problem of the mixture of the light coming back from X-arm and Y-arm can be mitigated by frequency shifting the two green lasers by 100 MHz or so.

1.9.3 Third Harmonics Demodulation

One way to get error signals of the central part insensitive to the arm resonance is a method called third harmonics demodulation (THD). In this scheme REFL port signal is demodulated at the third harmonics frequencies of the RF sidebands. The signal is produced by the beat between the second harmonics of the upper (lower) RF sideband and the first order lower (upper) RF sideband. Since both sidebands are not resonant to the arm cavities, when arm cavities are sufficiently close to the carrier resonance, these sidebands are not affected by the arm cavity motion.

Although the first and second harmonics of the RF sidebands are not resonant to the arm cavity, there is a contribution from the the third harmonics of the RF sideband to the THD signal. This is a

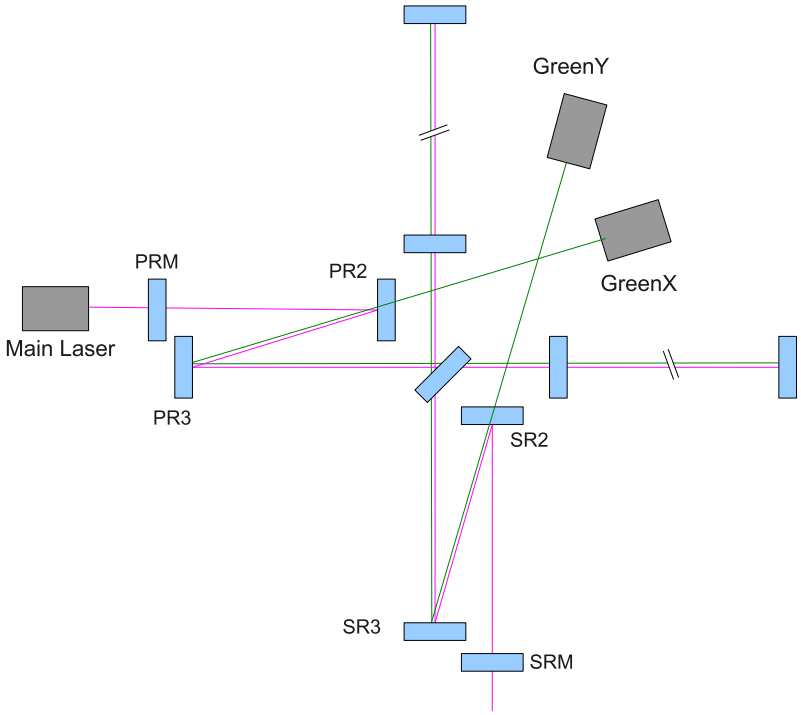

Figure 1.11: Conceptual configuration of the green laser pre-lock. Green lasers are injected from the back of PR2 and SR2. Two green lasers are phase locked to the main laser with a frequency offset of about 100 MHz.

beat between the carrier and the third harmonics of the RF sideband. Therefore, there is still inevitable coupling of CARM and DARM motion to the THD signals.

Figures 1.12 to 1.14 show the error signals of the central part plotted by varying the CARM offset from 2 nm to 0. The signals are almost insensitive to the CARM offset. However, MICH signal is largely affected by CARM when the offset is close to zero.

An advantage of THD is its simplicity. No additional modulator or Mach-Zehnder is necessary. We can try it by just adding PDs capable of detecting the third order harmonics. The PD for $3 \times f2 = 135\,\mathrm{MHz}$ may be challenging. However, since this PD is used only for lock acquisition, the noise requirement is not severe.

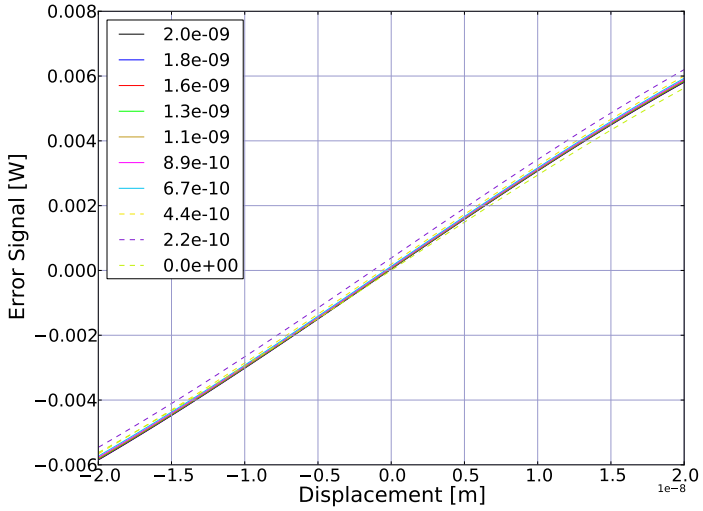

Figure 1.12: THD MICH error signal with various CARM offset. Signal port is REFL, demodulated at $3 \times f1$ in Q-phase.

1.9.4 Non-Resonant Sideband for Lock Acquisition

Another way to produce robust signals for the central part during lock acquisition is the use of a non-resonant sideband (NRS). The NRS is chosen not to be resonant to any part of the interferometer. So it serves as a stable local oscillator for signal generation.

The NRS error signals of the central part with changing CARM offset are shown in Figures 1.15 to 1.17. As expected, the signals are not affected by CARM at all. We used $f3 = 7 \times f_{\mathrm{MC}}$ as the NRS frequency for those plots.

The NRS scheme requires additional AM modulator to be introduced in the modulation stage. To avoid the generation of sub-sidebands, which interferes with the double demodulation, we also have to use a Mach-Zehnder to separate the AM path from the PM. This is a disadvantage of the NRS method. Since the NRS is only used in the lock acquisition phase, we do not need a large AM. We may also be able to close the AM path after the interferometer is locked, so that the Mach-Zehnder may not introduce excess noise to the laser.

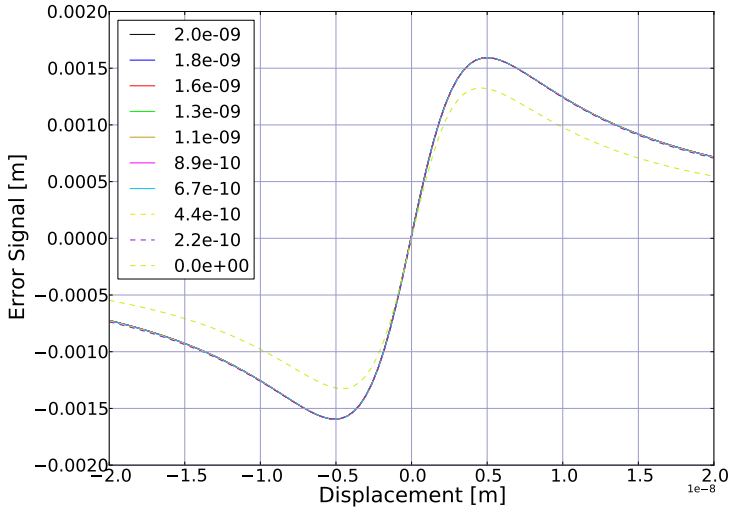

Figure 1.13: THD PRCL error signal with various CARM offset. Signal port is REFL, demodulated at $3 \times f2$ in I-phase.

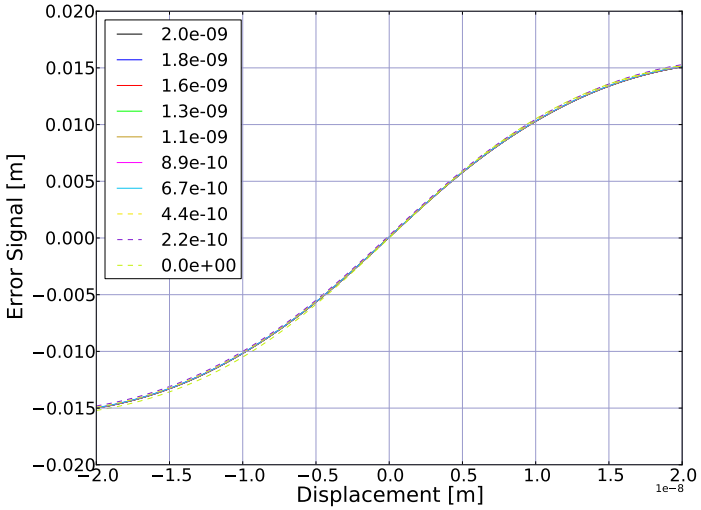

Figure 1.14: THD SRCL error signal with various CARM offset. Signal port is REFL, demodulated at $3 \times f1$ in I-phase.

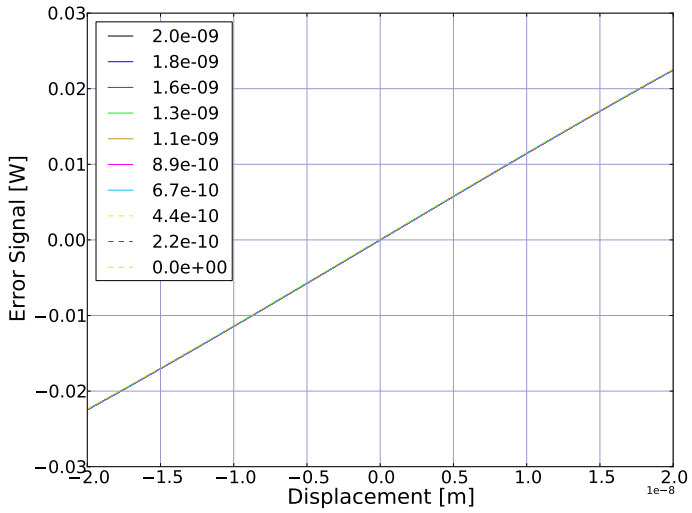

Figure 1.15: NRS MICH error signal with various CARM offset. Signal port is REFL, demodulated at $|f3 - f1|$ in Q-phase.

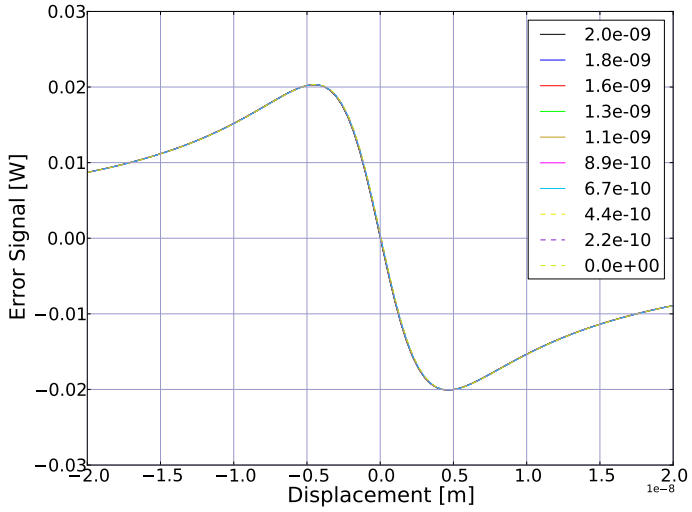

Figure 1.16: NRS PRCL error signal with various CARM offset. Signal port is REFL, demodulated at $|f3 - f2|$ in I-phase.

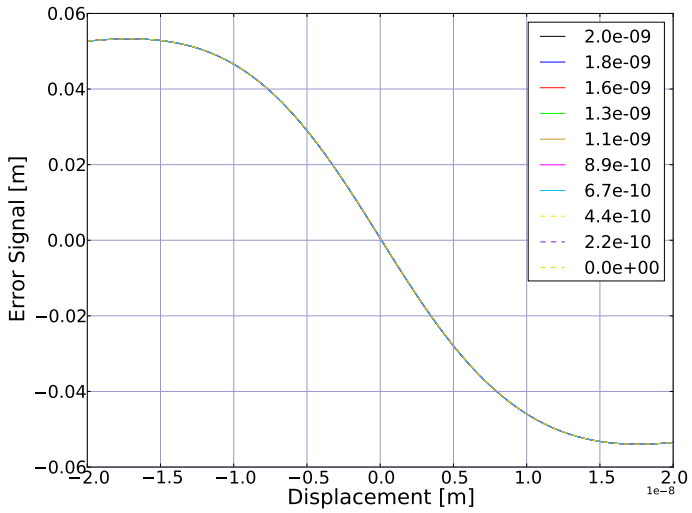

Figure 1.17: NRS SRCL error signal with various CARM offset. Signal port is REFL, demodulated at $|f3 - f1|$ in I-phase.

1.10 Schedule

The schedule of the main interferometer subsystem is shown in Tables 1.18,1.19 and 1.20.

Tasks	FY2011												FY2012												FY2013			
	4	5	6	7	8	9	10	11	12	1	2	3	4	5	6	7	8	9	10	11	12	1	2	3	4	5	6	7
Design																												
ASC																												
Folding Optimization																												
Simulated Plant Test																												
Linear Plant																												
Non-linear time domain plant																												
Digital Controller																												
Closed Loop Test																												
OMC																												
Requirement fix																												
LSC Design																												
ASC Design																												
Prototype Fabrication																												
Prototype Test																												

Figure 1.18: Schedule during the excavation and vacuum installation period

1.11 Prototype Test Plan

We do not plan to do a prototype experiment for the main interferometer. However, there have been several experimental tests of RSE interferometers. Particularly Japanese researchers have been involved heavily in the experiments at NAOJ and at Caltech 40m lab.

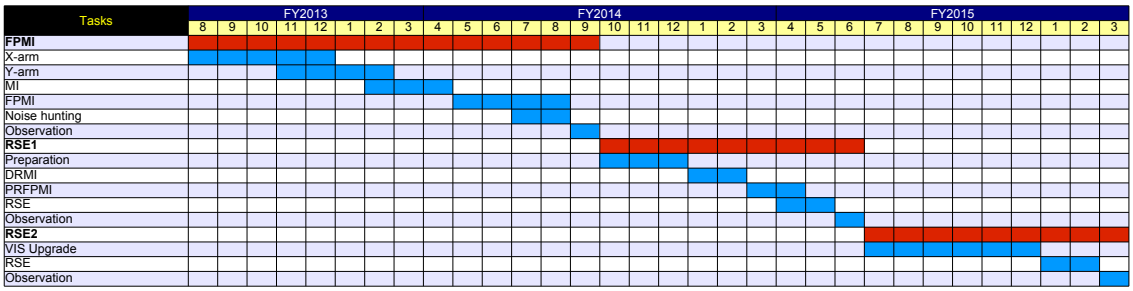

Figure 1.19: Schedule: FPMI, RSE1 and RSE2

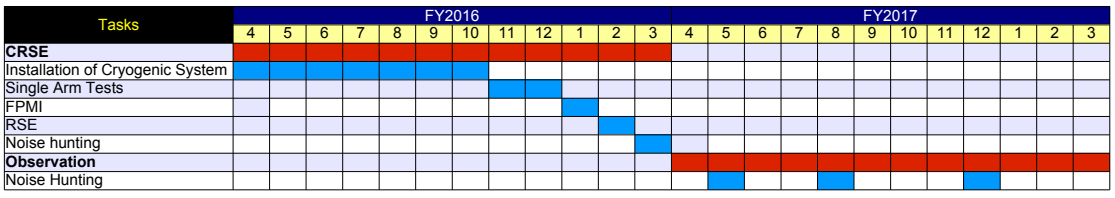

Figure 1.20: Schedule: Cryogenic RSE and Observation

Instead of real experiment, we will use computer simulations of the interferometer to predict the behavior of the interferometer and develop suitable control schemes.

Since the interferometer control will mostly be done by the digital system in LCGT, we can develop and test the interferometer control system without a real interferometer during the tunnel excavation period. The basic idea is to create a simulated plant of the LCGT interferometer in a computer. This plant accepts usual interferometer inputs, such as mirror actuator drives, laser frequency control, seismic noise etc. In response to those inputs, the simulated plant produces sensing signals. The simulation engine can be a simple linearized model of the interferometer around the operation point[3] or a more complicated time domain simulation codes, such as e2e. The simulated plant is connected to the digital controller to simulate the full closed loop system. The digital control system developed in this way can be used for the real interferometer by simply changing the connection to the simulated plant to real ADC/DACs. This way, we could save some commissioning time.

1.12 First Article Test Plan

Commissioning is the first article test for the main interferometer.

1.13 Installation/Adjustment Procedure

The physical installation of the main interferometer components will be done by other subsystems, such as suspension and mirror. After the initial installation of the mirrors, the distance between them (arm length, PRCL, SRCL, Schnupp asymmetry) have to be checked.

The cavity lengths are checked by measuring the FSR of the cavities. The Schnupp asymmetry can be measured by locking the arms one by one using the REFL port PDH signal, and measuring the difference of the optimal demodulation phases. The g-factor of the arm cavities can be measured by injecting a slightly mis-aligned secondary laser and check the frequency separation between resonances of the TEM00 mode and the TEM10 or TEM01 modes. The finesse of the arm cavities must also be measured.

After those measurements, the MC length should be fine adjusted to set the RF sideband frequencies at a desirable location in the FSR of the arm cavities. Then the length of PRC and SRC will be adjusted to resonate these sidebands. The ROC error of the PR3 (SR3) also has to be compensated by adjusting the distance between PR2 and PR3 (SR2 and SR3), keeping the overall PRC (SRC) length the same.

Commissioning is almost a synonym of adjustments to the interferometer. Therefore, the whole commissioning process is the adjustment process.

1.14 Risk assessment

- The arm cavity loss may be higher. In this case, the PRC becomes under-coupled. This is not acceptable. We may have to prepare several PRMs with slightly different reflectivities.
- The arm cavity loss might be smaller than expected. In this case, the carrier light power at REFL will increase. This will result in the increased shot noise for double demodulation and THD signals. However, as long as we use single demodulation signals for observation, this should not be a problem.
- The reflectivity mismatch of the two arm cavities may be too large. In this case, we have to add a large DARM offset to create strong enough DC offset light at the AS port and make the homodyne phase to the desired value.

[3] Optickle can be used to generate such a model

- The non-linearity of the SRC error signal when detuned may produce unwanted up converted noise. Although the up conversion noise was estimated to be not a problem from the predicted seismic noise and shot noise, it may still create wide side lobes around sharp noise lines.
- By detuning the SRC, the f1 sideband gets some phase rotation. This means the f1 no longer acts as a pure PM for the carrier. The result is large offsets in MICH and CARM (if f1 is used for CARM). This offset (in the order of nm for MICH and 10 pm for CARM) has to be canceled by electric offset.
- The design of the output mode cleaner has not yet studied in detail. Especially, the control schemes (length and alignment) have not decided yet.
- In the current folding design, the mode of the PRC is very sensitive to the ROC of PR3. We may have to change the distance between PR2 and PR3 by more than 10 cm if the ROC error of PR3 is large (about 1%).

Chapter 2

Design for iLCGT

2.1 Definition and scope of the Main Interferometer subsystem

The definition of the subsystem is the same as bLCGT.

2.2 Requirements

The requirement for the iLCGT main interferometer is to be able to operate a 3 km Fabry-Perot Michelson interferometer stably. The sensitivity is not specified as a requirement.

2.3 Interface

Interface items of iLCGT are almost the same as bLCGT. The only significant difference is the wedge angle of the ITMs. The requirements to the ITMs are listed in Table 2.1.

2.4 Optical Configuration

The optical configuration of iLCGT is a Fabry-Perot Michelson interferometer without recycling. Since iLCGT is on the pathway to bLCGT, the optical parameters are mostly the same as bLCGT. The PRM is replaced with a mirror blank with the HR coating replaced by AR. The mirror blank has the same ROC as the PRM of bLCGT to keep the spatial mode matching from the MC to the PRC. SRM will not be installed at this stage.

The arm cavity mirrors are made of fused silica instead of sapphire. All the other parameters are exactly the same as the bLCGT design.

2.5 Optical Layout

The optical layout of iLCGT is also generated by the python code. Since the ITM substrate is silica in iLCGT, the index of refraction is different from the sapphire mirror of bLCGT. To compensate for this, the wedge angle of the ITMs for iLCGT is different from the ones for bLCGT.

Parameter Name	Value	Comments
HR Reflectivity@1064 nm	99.6±0.01%	Power reflectivity
HR Reflectivity Mismatch @1064 nm	<0.05%	$\lvert R_{\mathrm{ITMX}} - R_{\mathrm{ITMY}} \rvert$
HR Reflectivity@532 nm	80±10%	ITM reflectivity must be smaller than ETM
HR loss@1064 nm	<45 ppm	Including diffraction and absorption
HR loss@532 nm	<1%	Including diffraction and absorption
AR Reflectivity@1064 nm	200(+100/-0) ppm	
AR Reflectivity@532 nm	<5%	
HR ROC	>500 km	As large as possible
HR ROC Mismatch between ITMX and ITMY	<10 km	
AR ROC	>500 km	As large as possible
AR Wedge Angle	0.335±0.002 deg	

Table 2.1: Input Test Mass Requirements for iLCGT

	DARM	CARM	MICH
AS_1I	1	1.7×10^{-3}	1.0×10^{-3}
REFL_1I	8.8×10^{-3}	1	1.3×10^{-4}
REFL_1Q	4.5×10^{-3}	5.5×10^{-5}	1

Table 2.2: Normalized Sensing Matrix of LSC for iLCGT. Each row is normalized by the diagonal element. The interferometer response was evaluated at 100 Hz to create this matrix.

2.6 Length Sensing and Control Scheme

All the degrees of freedom (DARM, CARM, MICH) are sensed by RF readout schemes. The sensing matrix is shown in Table 2.2. DC readout for DARM may be tested with iLCGT, but it is not the default plan.

2.7 Alignment Sensing and Control Scheme

We will use WFS for the alignment sensing of iLCGT. The sensing matrix is shown in Table 2.3. It can be diagonalized as shown in Table 2.4. Note that this diagonalization does not take into account the shot noise of different ports. In general, when taking a linear combination of signals from various ports, we should avoid using ports with poor shot noise, even at the expense of some signal mixing. This is still in our TO DO list.

2.8 Lock Acquisition Scheme

We plan to test the green laser pre-lock in iLCGT.

	CSOFT	CHARD	DSOFT	DHARD
REFL_2IB	-6.1×10^{1}	-2.8	-1.5×10^{-3}	1.1×10^{-2}
REFL_2IA	-3.2	-2.2×10^{1}	-2.9×10^{-2}	-1.4×10^{-3}
AS_1QB	-8.0×10^{-2}	-1.3×10^{-2}	2.7×10^{4}	4.4×10^{3}
REFL_1QA	2.7×10^{-3}	-4.7×10^{-4}	-1.4×10^{1}	1.8×10^{1}

Table 2.3: Sensing Matrix of ASC for iLCGT [W/rad].

	CSOFT	CHARD	DSOFT	DHARD
REFL_2IB	1	0	-8.7×10^{-5}	-1.8×10^{-4}
REFL_2IA	0	1	1.3×10^{-3}	8.7×10^{-5}
AS_1QB	-2.5×10^{-5}	3.4×10^{-6}	1	0
REFL_1QA	1.3×10^{-4}	-2.4×10^{-5}	0	1

Table 2.4: Diagonalized Sensing Matrix of ASC for iLCGT. The each row is normalized by the diagonal element.

2.9 Schedule

See section 1.10.

2.10 Prototype Test Plan

See section 1.11.

2.11 First Article Test Plan

Commissioning is the first article test for the main interferometer.

2.12 Installation/Adjustment Procedure

2.13 Risk assessment

- Commissioning time is extremely limited.

Appendix A

Reasoning Behind Parameter Choices

This section is to be written.

A.1 Arm Cavity Parameters

A.2 Recycling Cavity Length

A.3 Length Sensing Scheme

A.3.1 Alternative Schemes

Appendix B

Terminology

Table B.1: Terminology

DARM	Differential Arm Length	
CARM	Common Arm Length	
MICH	Michelson Part	L shaped part of the interferometer formed by BS and two ITMs
PRC	Power Recycling Cavity	
PRCL	Power Recycling Cavity Length	
SRC	Signal Recycling Cavity	
SRCL	Signal Recycling Cavity Length	
AS	Anti-symmetric port	
REFL	Reflection port	
POP	Pick-off in the Power Recycling Cavity	
POX	Pick-off at the ITMX	
POY	Pick-off at the ITMY	
Auxiliary DOF		Length degrees of freedom other than DARM
AM	Amplitude Modulation	
PM	Phase Modulation	
MC	Mode Cleaner	
MZ	Mach-Zehnder	

Appendix C

Contributors

Followings are the people contributed to the discussion of the main interferometer design.

Yoichi Aso (chair), Kentaro Somiya, Osamu Miyakawa, Yuta Michimura, Kazuhiro Agatsuma, Erina Nishida, Chen Dan, Daisuke Tatsumi, Tomotada Akutsu, Kiwamu Izumi, Koji Arai, Kazuhiro Yamamoto, Hiroaki Yamamoto, Masaki Ando.

Bibliography

[1] https://granite.phys.s.u-tokyo.ac.jp/svn/LCGT/trunk/mif/OptLayout/

[2] M. Evans, LIGO Document T070260.

[3] https://granite.phys.s.u-tokyo.ac.jp/svn/LCGT/trunk/mif/IFOmodel

[4] K. Somiya and O. Miyakawa, *Applied Optics*, **23** (2010) 4335

[5] J. Sidles and D. Sigg, *Phys. Lett. A*, **354** (2006) 167